

## RESEARCH ARTICLE

# Hillslope water tracks in the High Arctic: Seasonal flow dynamics with changing water sources in preferential flow paths

Michel Paquette<sup>1,2</sup>  | Daniel Fortier<sup>1,2</sup> | Warwick F. Vincent<sup>2,3</sup> 

<sup>1</sup>Department of Geography, University of Montreal, 520 Ch. de la Côte-Ste-Catherine, Montreal, QC H2V 2B8, Canada

<sup>2</sup>Centre for Northern Studies (CEN), Pavillon Abitibi-Price, Université Laval, 2405 rue de la Terrasse, Québec, QC G1V 0A6, Canada

<sup>3</sup>Department of Biology and Takuvik Joint International Laboratory, Université Laval, 1045, av. de la Médecine, Québec, QC G1V 0A6, Canada

## Correspondence

Michel Paquette, Department of Geography, University of Montreal, 520 Ch. de la Côte-Ste-Catherine, Montreal, QC H2V 2B8, Canada

Email: michel.paquette@umontreal.ca

## Funding information

Networks of Centres of Excellence program ArcticNet; Indigenous and Northern Affairs Canada; Northern Scientific Training Program; Natural Resources Canada; Natural Sciences and Engineering Research Council of Canada; Fond de Recherche du Québec-Nature et Technologie (FRQNT); Centre d'études nordiques (CEN); Canadian Foundation for Innovation; Canadian Northern Studies Trust; Canada Research Chair program

## Abstract

Preferential subsurface flow paths known as water tracks are often the principal hydrological pathways of headwater catchments in permafrost areas, exerting an influence on slope physical and biogeochemical processes. In polar deserts, where water resources depend on snow redistribution, water tracks are mostly found in hydrologically active areas downslope from snowdrifts. Here, we measured the flow through seeping water track networks and at the front of a perennial snowdrift, at Ward Hunt Island in the Canadian High Arctic. We also used stable isotope analysis to determine the origin of this water, which ultimately discharges into Ward Hunt Lake. These measurements of water track hydrology indicated a glacio-nival run-off regime, with flow production mechanisms that included saturation overland flow (return flow) in a low sloping area, throughflow or pipe-like flow in most seepage locations, and infiltration excess overland flow at the front of the snowdrift. Each mechanism delivered varying proportions of snowmelt and ground water, and isotopic compositions evolved during the melting season. Unaltered snowmelt water contributed to >90% of total flow from water track networks early in the season, and these values fell to <5% towards the end of the melting season. In contrast, infiltration excess overland flow from snowdrift consisted of a steady percentage of snowmelt water in July (mean of 69%) and August (71%). The water seeping at locations where no snow was left in August 2015 was isotopically enriched, indicating a contribution of the upper, ice-rich layer of permafrost to late summer discharge during warmer years. Air temperature was the main driver of snowmelt, but the effect of slope aspect on solar radiation best explained the diurnal discharge variation at all sites. The water tracks in this polar desert are part of a patterned ground network, which increases connectivity between the principal water sources (snowdrifts) and the bottom of the slope. This would reduce soil–water interactions and solute release, thereby favouring the low nutrient status of the lake.

## KEYWORDS

Arctic, isotopes, patterned ground, permafrost hydrology, polar desert, water track

## 1 | INTRODUCTION

Hillslopes are a basic unit of natural hydrological systems, and run-off-generating interactions between precipitation and geomorphological features are a fundamental process that determines hillslope flow paths. In periglacial areas, the active layer thermal regime restricts water infiltration and circulation to shallow depths, and the heterogeneous distribution of snow creates spatial and temporal variations in water supply (McNamara, Kane, & Hinzman, 1998; Woo, 1983; Woo, Heron, & Steer, 1981; Woo & Young, 2003). In addition, hydrological phenomena affecting shallow groundwater operate at a

faster rate in sloping terrain, mainly because of higher hydraulic gradients and flow velocities, and these rates can be exacerbated by either local or widespread high hydraulic conductivity materials (Quinton & Marsh, 1999; Woo, Yang, Xia, & Yang, 1994). This combination of variable water inputs, shallow flow paths, topography, and material properties can create preferential flow paths such as water tracks, which often dominate hillslope hydrology in periglacial regions.

Water tracks are subsurface flow pathways of diverse morphology, usually in permafrost areas, whose principal hydrological role is to carry snowmelt water and sometimes rainfall downslope as subsurface flow (Gooseff, Barrett, & Levy, 2013; Kane, Hinzman, Benson, &

Liston, 1991; Mcnamara et al., 1998; Rushlow & Godsey, 2017). Water tracks have been the object of study mostly in Alaska and Antarctica, yet they have been reported in other parts of the periglacial domain, albeit sometimes under other terminologies (Curasi, Loranty, & Natali, 2016; Nicholson, 1978; Woo & Xia, 1995). Their importance in the periglacial landscape extends beyond that of a simple hydrological pathway, as they play specific roles in heat transfer and active layer development (Gooseff et al., 2013; Hastings, Luchessa, Oechel, & Tenhunen, 1989; Levy & Schmidt, 2016; Paquette, Fortier, Mueller, Sarrazin, & Vincent, 2015; Paquette, Fortier, & Vincent, 2017), solute transport (Levy, Fountain, Gooseff, Welch, & Lyons, 2011), and nutrient and carbon cycling (Ball & Levy, 2015; Cheng et al., 1998; Mcnamara, Kane, Hobbie, & Kling, 2008; Oberbauer, Tenhunen, & Reynolds, 1991). They also play a role in the development of the landscape, acting as an immature drainage network (Mcnamara, Kane, & Hinzman, 1999), as moisture provider for slow mass wasting processes (Verpaelst, Fortier, Kanevskiy, Paquette, & Shur, 2017), or as indications of denudation by leaching of fine material (Paquette et al., 2017).

Water tracks in polar desert landscapes are known to be preferential pathways for the water flowing from snowdrifts towards the bottom of the slopes (Paquette et al., 2017). These pathways mainly take the shape of gravel lag conduits and patterned ground, playing a hydrological role similar to soil pipes by locally increasing underground hydraulic conductivity. Specifically at Ward Hunt Island, a high latitude location at the northern tip of Canada, water track networks have been identified as principal flow paths linking hillside snowdrifts to the ultraoligotrophic (Villeneuve, Vincent, & Komárek, 2001) waters of Ward Hunt Lake. Geomorphologically dependant flow paths and flow regimes greatly influence water quality and characteristics, exerting a fundamental control on limnological conditions (Quesada et al., 2006), and although the water track morphology has been described in detail, their hydrological regime remains to be investigated. Specifically, little is known about the degree of interaction between water track flow and soil water. The objectives of the present study were to determine the discharge regimes, including delivery time and flow generation mechanisms, and the origins of the water coming from water tracks and seeping at the bottom of a polar desert slope. Our overall aim was to define hydrological functioning of water tracks on hillslopes, and their role as the primary link between precipitation and downstream systems in the High Arctic polar desert environment.

## 2 | STUDY SITE

Northern Ellesmere Island is a partly glaciated, alpine landscape at the northern edge of the Canadian High Arctic. Aridity limited ice advance during the Wisconsinian, a portion of the landscape therefore pre-dates the last glacial maximum and could have escaped glaciations for as much as >400,000 years (Lemmen & England, 1992). Among these areas, Ward Hunt Island is located 6 km off the northern coast of Ellesmere Island (Figure 1). It features hills with rounded summits, and their slopes are mantled by patchy glacial drifts veneer and frost-shattered, colluvial debris. The studied hillslope is located at the foot of such a hill (Walker Hill, elevation: 436 m above sea level (a.s.l.), whose eastern slope follows a concave-up profile with slope angle values ranging from 29.5° in the upper middle slope to 3.5° at the toe. The middle section of the slope, just above the maximum change of slope and Holocene sea levels of  $\geq 62$  m a.s.l. (Lemmen, 1988), harbours two rows of annual snowdrifts which quickly become the only remaining snowmelt sources after a few days of thawing. The geology of Walker Hill is primarily carbonates (Trettin, 1991), and bedrock exposures are rare on the studied sections. Surface material is a patchwork of glacial drift and gelifracted bedrock. The mean annual air temperature is  $-17.8$  °C (1995–2016), with only July having a positive mean, of 1.5 °C (CEN, 2016). Further descriptions of the physiography, geomorphology, and ecology of Ward Hunt Island and of the hillslope in the present study are given in Vincent et al. (2011) and Paquette et al. (2017).

## 3 | METHODS

The lower slope of Walker Hill exhibits surface run-off and alluvial reworking of sediments at discrete locations, mostly at the front of snowdrifts and at the bottom of the slope, where water tracks merge and seepage occurs (Paquette et al., 2017). These locations were chosen to investigate hydrological regimes of water tracks, as the seepage allows direct water sampling and measurement of discharge. Measurements were performed for the greater part of the snowmelt season in 2013 and 2016, and some discrete measurement were also made in 2014 and 2015. A total of three cutthroat flumes were installed (A, B, and C, Figure 1); Seep A was positioned at the downslope end of a relatively flat wetland, where sorted polygons were the main surface landforms. Seep B was located where a network of water tracks merged and seeped, and Seep C was located at the front of a perennial snowdrift. The flumes

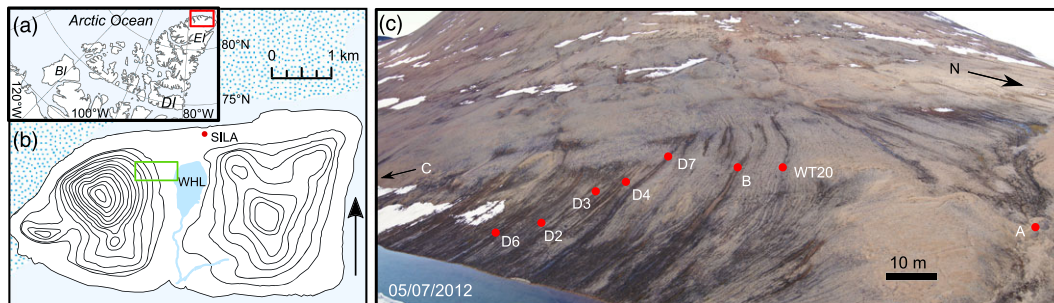


**FIGURE 1** (a) Location of Ward Hunt Island in the Arctic Archipelago. EI = Ellesmere Island; BI = Banks Island; DI = Devon Island. (b) Topography of Ward Hunt Island (30-m isolines), with location of the studied slope section. SILA = weather station; WHL = Ward Hunt Lake. (c) The lower slope of Walker Hill, showing the measurement sites. The picture was taken after an unusually warm early summer, and snowmelt was already well advanced

placed at those three locations were snugly fitted into the ground and equipped with a Hobo U20 water pressor sensor (accuracy of  $\pm 0.14$  cm; Onset, Bourne, USA). Water levels ( $h_u$ , cm) were obtained from absolute pressures through barometric compensation and were then used to calculate free flow discharge ( $Q_f$ ,  $\text{cm}^3 \text{s}^{-1}$ ) using the equation:

$$Q_f = K_f \cdot C_f \cdot h_u^{n_f}, \quad (1)$$

where  $K_f$  is a free flow correction factor calculated from the specific dimensions of the flume,  $C_f$  is the free flow coefficient, and  $n_f$  is the free flow exponent, both of which can be extracted from tables depending on the flume standard dimensions (Siddiqui, Lashari, & Skogerboe, 1996). Although care was taken that no water flowed underneath the flumes, which was successful at Seeps B and C, the coarse nature of the sediments at Seep A still allowed some subsurface flow. In 2016, another U20 was placed in a stilling well in the middle of a water track seepage (D6). Discharge values for this location were calculated using a rating curve obtained by the discrete measurements method detailed below ( $n = 16$ ,  $R^2 = .87$ ).

Discrete discharge measurements were used to monitor flow in other seeps of similar morphology to B (D2, D3, D4, and, D7) and in a vegetation-covered water track (WT20). They consisted of dilution and tracer gaging tests using a NaCl mixture and an electrical conductivity probe. Discharge ( $Q$ ) was then calculated as

$$Q = \frac{V \cdot C_i}{t \cdot C_m}, \quad (2)$$

where  $V$  is the volume of the injected solution,  $t$  is the amount of time taken for the passage of the tracer,  $C_i$  is the concentration of the injected solution, and  $C_m$  is the mean concentration of the slug (Whiting, 2005). These measurements were performed daily when possible (usually in the afternoon) and sometimes twice a day in the morning and in the afternoon.

Two pairs of stilling wells were installed, upslope from Seeps A and B, and equipped with a U20 water level logger. Each pair occupied a different position, either the "coarse" or "fine" grain-size sections of patterned grounds networks, where water flowed as determined in Paquette et al. (2017). As water is expected to travel preferentially through the coarse sections, the paired sensors provided flow direction, either towards the coarse or the fine sections. Thaw depth was measured 4 times at each well during the monitoring period, and wells were repositioned deeper when thaw depth increased. In the case of Seep B, wells were not placed directly upslope from the flume, as disturbances would have affected other experiments, but rather in the adjacent patterned ground subwatershed where soil pits were made previously (Paquette et al., 2017). The wells at Seep B could not therefore be used to monitor any water pulse through the system, as the specific source and the pathways would have differed at this site.

Meteorological variables were measured at the SILA weather station located on the north shore of the island (outside of the watershed) and recorded on a CR10X data logger (Campbell Scientific, Edmonton, Canada). Air temperature was measured with a thermistor in a solar radiation shield, snowmelt was measured as snow height change using a Sonic SR50 sensor (Campbell Scientific, Edmonton, Canada) positioned over a snowdrift, and incoming solar radiation was collected using a LI-200 (Li-Cor Biosciences, Lincoln, USA). Hourly solar radiation was corrected to account for the slope angle (mean =  $18.5^\circ$ ) and

aspect (mean =  $75.1^\circ$ ), both determined from the random sampling (5% of data points) of a digital elevation model of Walker Hill.

Water sampling for deuterium and  $^{18}\text{O}$  concentrations was performed discretely every few days in 2013 and for a few days in 2014 and 2015. In 2016, samples were taken at least twice a day, in the morning and in the evening (estimated time of high and low flow conditions) at Seep A, and often a third time at midday at Seep B. In order to measure the daily variation in water sources at Seep B, isotopes were sampled every hour for 24 hr in 2016. Precipitation was sampled by digging snow pits and collecting snow at 10-cm depth intervals.

Isotopic signatures of soil water were determined by melting ice in cores of the frozen active layer collected during mechanical coring operations, using a portable earth-coring system. Permafrost samples were collected the same way, by drilling to a maximum of 3-m depth in the ground. Cores were thawed in sealed and vacuumed plastic bags, from which water was then drained. Snowpack composition was sampled by digging snow pits in snowdrifts and by sampling every 10 to 20 cm. Fresh snow and rainfall samples were also collected during precipitation events, and the fallen amounts were measured using a metric rain gauge, read twice a day at 0700 and 1900 hr. All isotopic measurements were made with an LGR isotope analyser at the Facility for Biogeochemical Research on Environmental Change and the Cryosphere of Queen's University. Accuracy of the measurement was better than 0.25‰ for  $^{18}\text{O}$  and 1.5‰ for deuterium.

The relative contributions from snowmelt and soil water (active layer ice) to discharge were estimated using a two-component separation technique (Carey & Quinton, 2005; Sklash & Farvolden, 1979) using  $^{18}\text{O}$  as a tracer. The fractional contribution from each source was calculated as

$$\frac{Q_1}{Q_T} = \frac{(C_T^{t_1} - C_2^{t_1})}{(C_1^{t_1} - C_2^{t_1})}, \quad (3)$$

where  $Q_1$  is the contribution from snowmelt,  $Q_T$  is the total run-off,  $c_T$  is the concentration of the observed tracer in the run-off, and  $c_1$  and  $c_2$  are the concentrations of the tracer in snowmelt and in active layer ice, respectively. Uncertainty resulting from Equation 3 ( $W_{f_1}$ ) can be attributed to analytical error in the measurement of  $c_T$  and to the standard error of the mean calculated for each end member and was calculated by applying the method described by Genereux (1998):

$$W_{f_1} = \sqrt{\left[ \frac{C_T - C_1}{(C_1 - C_2)^2} W_{C_2} \right]^2 + \left[ \frac{C_2 - C_T}{(C_T - C_2)^2} W_{C_1} \right]^2 + \left[ \frac{1}{(C_1 - C_2)} W_{C_T} \right]^2}, \quad (4)$$

where  $W$  represents the uncertainty for the variables specified by the subscripts. Part of the snowmelt water refreezes during the snowmelt process, and isotopic fractionation will therefore occur, modifying the values of the modelled contribution. The relationship between initial water  $\delta^{18}\text{O}$  isotopic composition ( $\delta_o$ ), the composition of the ice ( $\delta_i$ ), and of the residual water ( $\delta_w$ ) freezing in an open system was calculated as in Lacelle (2011):

$$\delta_i = \delta_o + \ln(\alpha_{i-w}) \cdot 1000 \cdot \ln f + \ln(\alpha_{i-w}) \cdot 1000, \quad (5)$$

$$\delta_w = \delta_o + \epsilon_{i-w} \ln f, \quad (6)$$

where  $\ln(\alpha_{i-w}) \cdot 1000$  equals 3.018 for  $\delta^{18}\text{O}$  and 15.228 for  $\delta^2\text{H}$ , whereas  $\epsilon_{i-w}$  equals 3.022 and 15.345, and  $f$  is the residual fraction of water

(Lacelle, 2011; O'Neil, 1968). Statistical analysis was performed using R 3.1.1 (R Core Team, 2014), and wavelet analysis of the bivariate time series was accomplished using the WaveletComp package (Roesch & Schmidbauer, 2014).

## 4 | RESULTS

### 4.1 | Discharge regimes

The discharge regimes of all monitored sites showed a diurnal cycle that began a few days after the onset of snowmelt (Figures 2 and 3). Positive air temperatures led to rapid rises in discharge in all seeps, whereas the returns to freezing temperatures were associated with extended recessions. The year 2013 was a relatively cold year when comparing with Ward Hunt climatic conditions (Paquette et al., 2015, Figure 2a). The melting season began in late June, but steady  $>0$  °C temperatures only occurred starting in mid-July. In contrast, summer 2016 began quite early and remained steadily warmer, except mainly for a blizzard that occurred from June 23 to 25, which filled up all the flumes and the seeps with snow and interrupted water flow (Figure 3a,d,h). Because of warmer climatic conditions, accumulated snowmelt had already reached more than 100 cm on July 1, compared with 15 cm on the same date in 2013 (Figures 2b and 3b).

The timing and magnitude of flow conditions differed between the two years. In 2013, steady discharge only began on July 6, and peak discharges at all sites were registered during the night of July 16 to July 17. Prior to this period, the melting season was steadily interrupted by cold spells where snowmelt was minimal (Figure 2c,d).

In contrast, 2016 had steady discharge very early on, starting on June 10 at Seep A (Figure 3i) and on June 9 at Seep B (Figure 3h), and both reached their peak discharge a few days later, on June 13. The flume at Seep C remained covered by snow until later in June but also began registering high discharge values early in the season as compared with 2013 (Figures 3h vs. 2d). Its highest discharge, however, was recorded much later than in the other seeps, on July 3, and was coincident with a peak of air temperatures above 10 °C for several hours.

Greater overall daily discharge was recorded in 2016, with daily peak discharge regularly exceeding those occurring in 2013 (Table 1). Maximum discharge was reached in 2013 at Seep A, which had by far the largest discharge measurements of all seeps, ranging about an order of magnitude above the others. Seep B saw the opposite of Seep A, as the largest discharge registered in 2013 was exceeded on seven occasions during 2016, and Seep C recorded similar maxima in both years. The 2016 monitoring period was long enough and had the appropriate timing to record flow recession to base levels or to the end of flow in Seeps A, B, and D6 (Figure 3h,i).

Discretely measured discharge of active seeps located around B and D6 provided an account of the spatial variation (Figure 3j). Seeps typically possessed discharge values smaller than those of Seep B, which was also the first to become active in the season. D4 showed the greatest relative value early in the season of  $0.40 \text{ L s}^{-1}$ , followed closely by D3 and D7. Seep D2 registered some discharge early in the season but quickly dried up before the June 23 snowfall. WT20, short for water track 20, did not seep but rather flowed through a gravel conduit underneath a cover of mosses (see Paquette et al., 2017 for details on water track morphology). It maintained low discharges (mean of  $0.03 \pm 0.016 \text{ L s}^{-1}$ ) even during warm events but

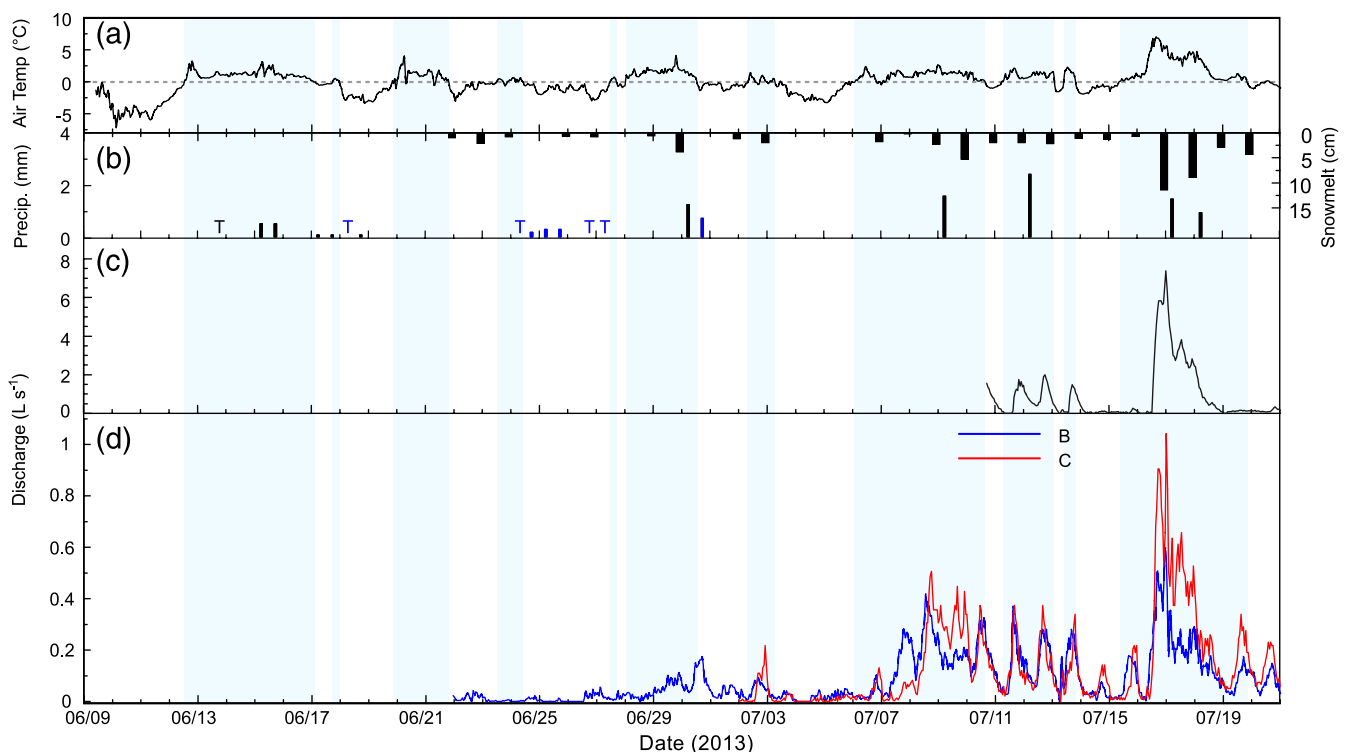


**FIGURE 2** Meteorological and hydrological data from 2013. Blue areas have positive air temperatures, whereas white areas are below freezing. (a) Air temperature; (b) rainfall (black), snowfall (blue) and daily snowmelt, T = trace; (c) discharge in Seep A; (d) discharge in Seeps B and C

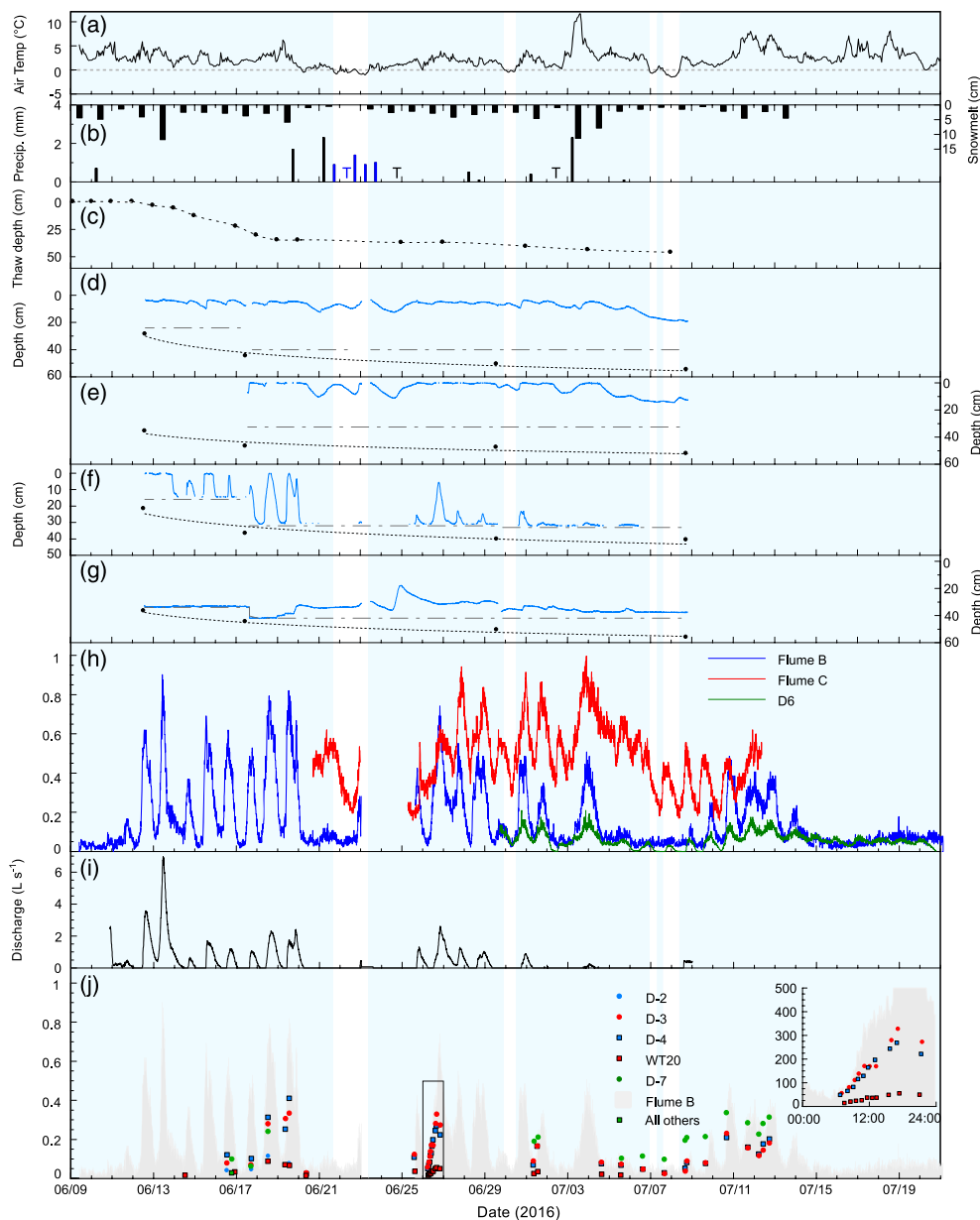


**FIGURE 3** Meteorological and hydrological data from 2016. Blue areas have positive air temperatures, whereas white areas are below freezing. (a) Air temperature; (b) rainfall (black), snowfall (blue) and daily snowmelt, T = trace; (c) active layer thawing front depth; (d) water level (blue line), thaw front depth (dotted line and dots), and depth to the bottom (broken line) of a well upslope from Seep A, in the fine section of patterned ground; (e) same as (d) but in the coarse section of patterned ground; (f) water level (blue line), thaw front depth (dotted line and dots), and depth to the bottom (broken line) of a well, in a water track upslope from Seep B; (g) same as (f) but in the intertrack section; (h) discharge in Seeps B and C and at Site D6; (i) discharge in Seep A; (j) discharge in other seepage sites, the rectangle is enlarged in the insert on the right

**TABLE 1** Discharge values (in  $L s^{-1}$ ) in 2013 and 2016

Seepage site	Mean		Maximum	
	2013	2016	2013	2016
A	0.93	0.89	7.39	6.97
B	0.06	0.16	0.47	0.90
C	0.13	0.48	0.94	1.00
D6		0.06		0.21

reached its maximum capacity ( $0.06 L s^{-1}$ ), and water was at times seen flowing on top of the vegetation. Flow in D7 increased later in the season, and its highest levels ( $0.33 L s^{-1}$ ) were recorded during the second week of July. The recorded values even surpassed the discharge from

Seep B during this period, when it became the most active of all seeps in the area. The monitoring of D3, D4, and WT20 performed over 15 hr on June 26 showed a rise of the hydrograph simultaneous with Seep B, followed by recession.

The timing of daily maximum and minimum discharges vary only slightly between sites, unlike the discharge amplitude which can vary by more than an order of magnitude. All locations typically experienced low flow conditions in the early morning and peaking flow levels late in the afternoon or during the evening. Iterative, multiple regressions were performed on 2016 discharge measurements, using air temperatures and slope-corrected solar radiation as explanatory variables (Table 2). The iteration consisted of using discharge values with a delay of between 0 and 23 hr, to correct for a potential time delay between

**TABLE 2** Partial correlation ( $r$  values) between discharge at each seepage site and meteorological variables. Delays of 0 to 23 hr were applied to discharge measurements

Meteorological variable		Partial correlation coefficient ( $r$ )			
		A	B	C	D6
Air T	Min	.09	.03	.31	.23
	Max	.29	.25	.54	.53
	Mean	.19	.13	.47	.43
	SD	.07	.09	.07	.09
	Delay <sup>a</sup>	7	6.5	6	10
Radiation	Min	-.14	-.28	-.40	-.24
	Max	.43	.48	.24	.42
	Mean	.17	.13	-.05	.10
	SD	.20	.27	.21	.24
	Delay <sup>a</sup>	11	12	12	15.5

<sup>a</sup>delay in hours at maximum correlation.

environmental variables and discharge. All data showed a relatively small standard variation in the Pearson correlation coefficient ( $r$ ) for air temperature compared with radiation. A and B showed a discharge with a stronger correlation to radiation, whereas C and D6 variations were more correlated to air temperatures. Overall, discharge is always positively related to air temperatures, while the diurnal radiation regime on the slope created a time-sensitive correlation with discharge. Wavelet analysis of the time series measured the strength of the diurnal signals of the variables. Air temperatures did not vary according to a 24-hr period (average  $p$  value of .358), but radiation showed a strong diurnal variation (average  $p$  value < .05), caused mainly by the effect of slope angle and aspect. Cross-wavelet analysis of radiation and discharge showed a strong coherence over daily periods, most of all when temperatures were above 0 °C (Figure 4). The cross analysis also provided a measure of time delay when both

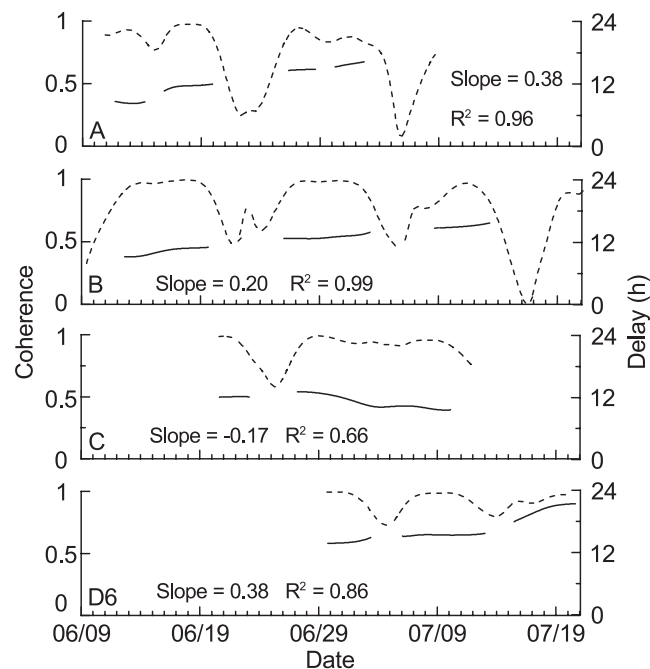


**FIGURE 4** Coherence (dotted line) between solar radiation and discharge variation in Seeps A, B, C, and D6 and delays (full line) between their respective cycles, as determined from wavelet analysis. Also shown are the slope and coefficient of determination ( $R^2$ ) applied to the delay

time series cycles best overlapped. Time delays were over 6 hr in every case and increased during the season in all locations except C. The delays reached more than 16 hr in A, 14 hr in B, and more than 18 hr in the case of D6. At Seep C, time delays went from 12 to approximately 8 hr at the end of the monitoring period.

Wells installed upslope from Site B showed contrasting water level behaviour between the coarse and the fine sections of the patterned grounds (Figure 3f,g). The coarse section (water track section, Figure 3f) exhibited water levels that behaved almost identically to the hydrograph of Seep B. They peaked and collapsed rapidly during diurnal episodes, with the highs occurring at a mean of 104 min after B peaked ( $\sigma = 59$ ,  $n = 18$ ). This delay could be an artefact caused by placing the well upstream another subwatershed next to B, to avoid disturbing sediments concentrations which were monitored in another study. Water levels often rose to the surface or near surface early in the season, but peaks became rarer and weaker as the season went on. In the fine section (intertrack section, Figure 3g), levels were much steadier, rarely rising closer than 0.3 m from the surface. Small amplitude peaks sometimes followed the main peaks in the coarse well, but the biggest peak occurred just after the onset of snowmelt following the June 23–25 snowfall.

The wells upslope from Seep A had a more correlated response between them (Figure 3d,e). The coarse sediment well (Figure 3e) had the most variable behaviour, with amplitudes exceeding those in the finer sediment well (Figure 3d). Its level often rose to the surface during high discharge periods, and the rise occurred slightly earlier than in the finer well. Both wells maintained a high water table throughout the monitored period, which had begun to drop by the end of the monitoring record.

## 4.2 | Water isotopes

Our isotopic measurements of snowpack and collected precipitation are the only recent values that can be used to establish a local meteoritic water line (LMWL) for Ward Hunt Island and vicinity. The Global Network for Isotopes in Precipitation database includes  $\delta^{18}\text{O}$  and  $\delta\text{D}$  values for monthly means at Alert, Nunavut, spanning 5 years from 1989 to the end of 1993 (International Atomic Energy Agency/World Meteorological Organization, 2017), providing an LMWL of  $\delta\text{D} = 7.68 \pm 0.12 * \delta^{18}\text{O} + 3.37 \pm 3.82$  ( $n = 58$ ,  $r^2 = .99$ ). Rainfall may be more frequent at Alert than at our site, as total June–July precipitation averaged 42 mm at Alert but only 9 and 9.6 mm in 2013 and 2016, respectively on Ward Hunt Island. The reduced major axis regression calculated for the Ward Hunt LMWL was  $\delta\text{D} = 7.83 \pm 0.23 * \delta^{18}\text{O} + 1.15 \pm 6.24$  ( $n = 55$ ,  $r^2 = .95$ ). The slope of the ordinary least squared regression was not significantly different from the global meteoritic water line (Craig, 1961,  $F$  value = 1.81,  $p = .182$ ) or from the LMWL of Alert ( $F$  value < 0.01,  $p = .952$ , Figure 5).

Water stable isotope values for  $\delta^{18}\text{O}$ ,  $\delta\text{D}$ , and  $d$ -excess of precipitation and ground ice are presented in Table 3. Permafrost ice had the heaviest ratios, close to sea water in some cases, followed by rainfall, active layer ice, and snow. Snow and active layer ice isotopic compositions were used for end-member values in the mixing model, as rainfall amounts were small and permafrost ice, by definition, could not be a contributor of run-off before the active layer has thawed completely. They were applied to isotopic compositions, as shown in Figure 6, which combines all samples of surface run-off taken between

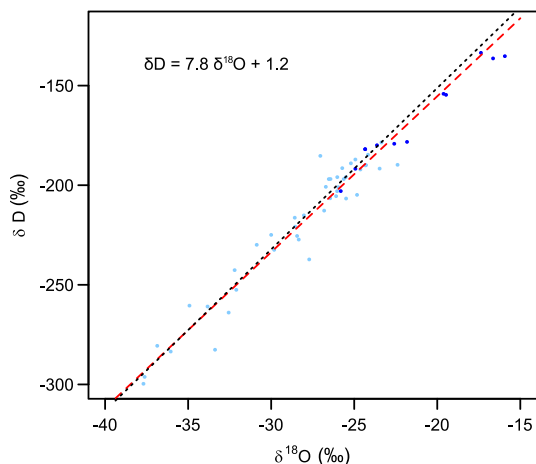


**FIGURE 5** Isotopic composition of precipitation on Ward Hunt Island displaying snowfall (light blue), rainfall (dark blue), the global meteoritic water line (black dotted line), and the local meteoritic water line (red broken line)

2013 and 2016. Standard error of the mean for snow (0.63) and active layer ice (0.35) along with the average analytical error of the samples (0.15) amounted to uncertainty values averaging ( $\pm$ standard deviation) 8.0% ( $\pm$ 2.2%). A seasonal trend is visible in all locations, as June values plot much closer to the snow mean end member, whereas July and August values plot progressively closer to the active layer ice average ratio, even surpassing it during low flow conditions in August 2014, a few days prior to freeze back. Samples plot mostly along or slightly to the left of the LMWL, except for Seep A samples which plot on the evaporative side of the line. Two-component mixing results for

Seep B are presented in Figure 7 as fractions of snowmelt contribution to discharge. High values with large variation are found early in the season, as snow is still present in the vicinity. A significant ( $F$  value = 285.6,  $p < .001$ ) decreasing trend in direct snowmelt contribution appears as the thawing season progressed and as snowdrifts became the only contributors of snowmelt, and late data suggest an increasing contribution from soil water or active layer ice (Figure 7a). Details of a 60-hr period including the hourly sampling period did not show any clear trend that can be associated with either the rise or fall of discharge (Figure 7b). The mixing model results for all analysed seeps, combining samples taken from 2013 to 2016, are presented in Table 4. All seeps showed a drop of snow contribution during the year, except for Seep C which still possessed relatively large Q1/QT values even in early August.

## 5 | DISCUSSION

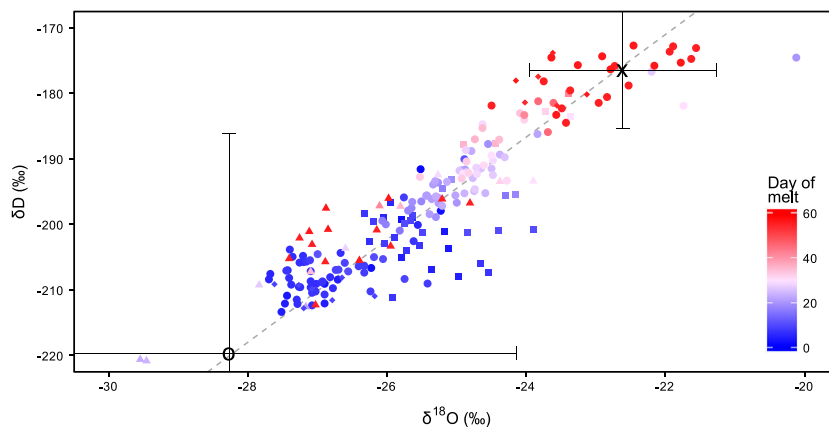
### 5.1 | Hydrological regime of water tracks

The water track seeps on Ward Hunt Island exhibited large diurnal variations in discharge but, except for Seep A, did not show any pronounced seasonal peak. Snowmelt water delivery in the seeps was dependant on air temperature, but the diurnal variation in discharge appeared to be controlled by the hourly variations in incident solar radiation, indicating the importance of slope aspect on snowmelt at high latitudes when summer temperatures hover just above 0 °C. In addition to strong diurnal cycles, the seeps did not return to baseflow conditions; instead, the recessions were interrupted by a new discharge

**TABLE 3** Measured isotopic composition of water sources at Ward Hunt Island

Source	n	$\delta^{18}\text{O}$				$\delta\text{D}$				<i>d</i> -excess			
		Mean	SD	Min	Max	Mean	SD	Min	Max	Mean	SD	Min	Max
Precipitation													
Rain	12	-21.4	3.5	-25.8	-15.9	-167.5	23.7	-203.0	-133.5	3.5	6.5	-7.8	12.8
Snow	43	-28.3	4.1	-37.7	-22.4	-219.7	33.5	-299.7	-178.5	6.5	8.9	-15.6	31.0
Soil water													
Active layer ice	15	-22.6	1.3	-24.6	-19.1	-176.4	9.0	-195.3	-156.7	4.5	4.5	-4.2	10.8
Permafrost ice	83	-16.2	7.1	-27.1	-1.2	-124.9	55.1	-203.7	-30.9	4.4	8.6	-30.7	27.1

**FIGURE 6** Isotopic composition of surface run-off between 2013 and 2016. Colours depend on sampling day, starting from June 10 (the earliest run-off recorded). Sites are represented by point shape. Seep A: square; Seep B: filled circle; Seep C: triangle; Others: diamond. The O and X are snow and active layer ice, respectively, with standard deviations, the end members for the mixing model



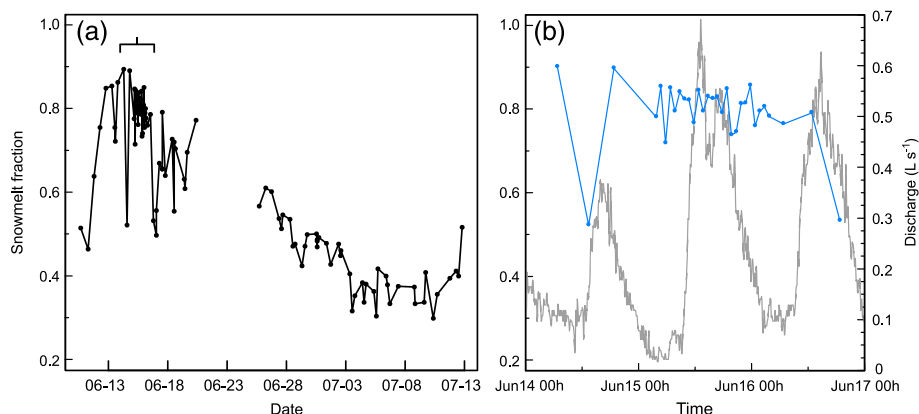


**FIGURE 7** Mixing model results in Seep B, showing the relative contribution of snowmelt to total discharge. (a) Seasonal pattern with timing of the hourly sampling period; (b) evolution of the contribution (blue) and of discharge (grey) during a 60-hr period, including a 24-hr period of hourly sampling

**TABLE 4** Monthly proportion of snowmelt water (Q1/QT) in run-off for each seep. Values include all years

	June				July				August			
	Mean	SD	Min	Max	Mean	SD	Min	Max	Mean	SD	Min	Max
Seep A	0.49	0.12	0.23	0.66	0.24	0.12	0.13	0.4	-	-	-	-
Seep B	0.66	0.2	0.34	0.9	0.33	0.12	<0	0.52	0.04	0.14	<0	0.33
Seep C					0.71	0.33	0.22	>1	0.69	0.06	0.39	0.85
All seeps (11)	0.77	0.27	0.51	0.89					0.20	0.09	0.08	0.30

event when incident radiation rose again. The influence of slope characteristics on energy input has long been identified as important for snowmelt production (Dunne & Black, 1971), however, Hardy (1996) noted a less prominent role of radiation compared with air temperature for discharge in nearby Taconite Inlet (inflow to Lake C2). Our findings indicate that a combination of steep topography and slope aspect can play a similar role to sunset in the energy balance at polar latitudes. The importance of solar radiation for snowmelt production had been similarly shown by measurements and models for other high latitude locations (Hoffman, Fountain, & Liston, 2014; Woo, Yang, & Young, 1999; Young & Lewkowicz, 1990; Young, Woo, & Edlund, 1997), as well as in alpine conditions in the subarctic (Quinton, Carey, & Goeller, 2004). It has also been demonstrated in boreal forest and tundra environments (Dunne, Price, & Colbeck, 1976; Hamlin, Pietroniro, Prowse, Soulis, & Kouwen, 1998), with a day–night regime. Based on the classification of northern hydrological regimes by Church (1974), water tracks showed a proglacial regime but within a nival catchment. Seep A was more similar to a nival regime, as it peaked intensely during both season. The reaction of individual seeps to the production of snowmelt varies, with three distinct mechanisms for run-off generation: saturation overland flow (return flow), throughflow (or pipe flow), and infiltration excess overland flow (Hortonian overland flow).

## 5.2 | Flow regime in sloping sections: Throughflow

In Seep B, pulses of water transited through the coarse sections of patterned ground with only minimal interaction with surrounding soils, where fluctuations in water table were muted. This preferential flow path was also suggested by the absence of a pattern in the isotopic composition of run-off as the hydrograph rose and fell during a 24-hr period. In addition, the mixing model results showed a strong event water component, especially early in the season. This type of flow is similar to throughflow and pipe

flow, and these were likely the dominant mechanisms of flow generation in the water track networks leading to Seep B. Because D6 and other seeps (D3, D4, D7, and WT20) behaved similarly, it may be that all the lower slopes seeps and their water track networks behaved in the same way. However, as was shown by the delay between water pulses in Seep B and its wells, the exact timing and intensity could vary depending on the water track network configuration and location. When water flowed preferentially in coarse material of a hydraulic conductivity up to seven orders of magnitude greater than the surrounding soils, it could flow through the slope with little dependence on antecedent moisture conditions in these surrounding soils. The downstream movement of water in the fine-grained portion is limited, however, because of the extremely low hydraulic conductivity of the soil ( $10^{-5} \text{ m d}^{-1}$ ). The moisture in this portion of the ground cannot contribute to the downstream system, except if it was to return to the coarse-grained section when snowmelt inputs (and hydraulic head) diminish in the coarse section. This did not seem to occur in the wells at Seep B. These water tracks might therefore be considered as losing streams even before they emerge, as they contribute to local groundwater recharge instead of depending on groundwater levels to be able to flow.

Similar underground stream-like flow is known in alpine and periglacial landscapes. On steep and bare alpine slopes underlain by permafrost, the presence of gelifracts and coarse slope deposits can favour infiltration and rapid subsurface flow (Woo et al., 1994). Large spatial variations in hydraulic properties of soils have also been documented in periglacial areas in the past, notably by Hodgson and Young (2001) and by Quinton, Gray, and Marsh (2000) and Quinton and Marsh (1998) who found a three- to six-fold increase in  $k$  values in interhummock areas. Similar to the data from the coarse sediment well at Seep B (Figure 3f), these areas were also highly responsive to daily variations in snowmelt and were by far the greatest contributors of snowmelt water at the plot scale. However, the run-off generation

process was different in Seep B than in these locations, where a water table rise was necessary in order to activate these preferential flow paths of highly conductive peat.

### 5.3 | Flow regime in flat areas: Saturation overland flow

Seep A rarely exhibited continuous flow; its discharge regime rather indicated a fill and spill behaviour, or a return flow produced by saturation overland flow, much like in southern low-lying wetlands. This explains the relatively low direct contribution of snowmelt to discharge, which showed a good amount of mixing with pre-event water even early in the season. The relatively flat, sorted polygon network upstream from the seep location experienced elevated water tables prior to discharge events. The polygonal network experiencing water table fluctuations acted as a variable source area as defined by Dunne, Moore, and Taylor (1975). The shallow gravel pathways of the coarse-grained portions of the patterned ground network formed the preferential drainage network, which was mainly underground as is usually the case for water tracks. In 2013, the extended low temperatures caused a lack of sufficient water input from the upslope snowdrifts, preventing flow conditions from filling the network and producing run-off. Flow ceased completely during the season, as the thawing of the active layer increased the amount of water necessary to saturate the area. The different flow dynamics between these water tracks and those upslope from Seep B and other seeps could be explained by the low slope of the area ( $<3^\circ$ ) compared with the other networks ( $<9.7^\circ$ ), which prevented the formation of a large hydraulic gradient.

The conceptual framework for run-off generation for Arctic tundra landscapes described by Quinton and Marsh (1999), Carey and Woo (1999, 2001), and Carey (2003) could extend to this area. In our case, however, the interhummock peat network of their framework is replaced by the gravel networks of the polar desert polygonal terrain. This polyvalence of their framework underscores the hydrological importance of microtopography and soil surface properties, even in very different periglacial landscapes.

### 5.4 | Flow regime in front of snowdrifts: Infiltration excess overland flow

Seep C, located at the front of a large perennial snowdrift, had a unique behaviour among the monitored seeps. It showed the greatest annual variation in mean discharge, but maximum discharge remained similar in 2013 and 2016. In addition, it showed a relatively high correlation between discharge and air temperature while also maintaining a high amount of event water contribution during late summer and a diminishing delay between maximum radiation and maximum discharge. This hydrological signature indicates that the direct link with the event water source (the snowdrift) increased as the season progressed, indicative of infiltration excess overland flow. A negative slope relationship for the delay against melt season progression was also measured by Dunne et al. (1976), Lewkowitz and French (1982), and Lewkowitz and Young (1990a) who observed that thinner snow covers had the fastest response time to daily maximum energy input,

as meltwater waves take less time to cross thinner snow covers and can create more efficient flow pathways during the season. Seep C showed a contrasting pattern, with the negative slope of its delay between maximum energy input and maximum discharge being opposite to that measured in the other seeps, where delays increased as the season progressed. The steady high proportion of event water in Seep C throughout the season also differed from the other seeps, which registered a diminishing contribution of event water over the course of the season. The increased lag in other seeps could be explained by the increased thickness of the active layer, which obstructs event water flow and force it to travel through less conductive, sandier sediments at depth. It could also result from the increased distance to snowdrifts, as snowdrifts on the lower slopes of Walker Hill melted before snowdrifts at higher altitudes, further delaying the arrival of the meltwater wave.

### 5.5 | Ground ice contribution to run-off

Water in each of the seeps (except in Seep C) had an isotopic signature close to that of active layer ice late in the season, and some seeps began discharging again in August 2015, when snowdrifts had already disappeared for a few days. These waters probably came from the thawing of the ice-enriched transient layer, as defined in Shur, Hinkel, and Nelson (2005). Summers were colder in 2013 and 2014 (55.2 and 55.3 melting degree days, respectively; CEN, 2016), and no seepage was detected during fieldwork in August 2014. These summers would have increased transient layer ice content, due to a thinner active layer, as is usually the case during colder years (Shur, 1988). In contrast, 2015 had nearly twice as many melting degree days (105.1), which should have caused the melting of some of the ice in the transient layer.

Ground ice is usually not identified as an important contributor to streamflow in polar desert (Woo & Steer, 1983). However, late-season ionic enrichment of streamflow has been measured and attributed to ground ice melt in at least one other High Arctic locations (Lamhonwah, Lafrenière, Lamoureux, & Wolfe, 2017). In addition, similar late-season seeps in the McMurdo Dry Valleys, Antarctica, had also been attributed to the melt of ground ice, which was initially formed during snowmelt periods in colder years (Harris, Carey, Lyons, Welch, & Fountain, 2007). Overall, even without the late summer contributions of ground ice, seeps and water tracks that were not in the downslope vicinity of a snowdrift experienced a modification in their contributing source during the season. This indicates that ground ice was present in the active layer on the coarse, steep slopes of this polar desert. An extended warm season would therefore increase water availability, reducing water stress for plants and increasing inputs into the lake.

### 5.6 | Mixing model uncertainties

Isotopes are one method of performing hydrograph separation to measure event water contribution but are subject to known shortcomings. In regular hydrograph separation, "new" water will usually come from a time-specific rainfall event and will mix with the "old" water present in the soil just prior to the beginning of the event. In our case, the definition of event or new water and pre-event or old water is not straightforward,

because every day produces an event, yet 24-hr old water does not fall clearly in the old water category. It is possible that a fraction of snowmelt water remains in the soil and is only mobilized after a day or two or during low flow period, yet because of the low potential for evapotranspiration caused by thin or absent vegetation cover and by low energy inputs (temperatures and radiation) between events, this water would possess an isotopic composition close to snowmelt water and might not be detected as Pre-event water. This rationale justifies the construing of Pre-event water as water present in the soil during freeze back, that is, active layer ice.

The only indication of a potential evaporative effect was from the data at Site A, which plotted either close to or clearly to the right of the LMWL. These individual points taken through multiple events cannot be used to create an evaporation line, as they are not sampled in a standing water body and are separated by various inputs of event water, which might not possess the same original isotopic composition. This interpretation however is consistent with the fill and spill behaviour indicated by the hydrograph shape and by the wells data and suggests an extended transit time for meltwater compared with other seeps measured in this study. In the case of Seep A, identification of any event water is less clear, as the  $\delta^{18}\text{O}$  values of snowmelt were likely modified during its transport as groundwater.

Another difficulty in interpretation is that snowmelt signature is not equal to the signature of the snowpack or to fresh snow. The  $\delta$  D to  $\delta^{18}\text{O}$  relationship of the snowmelt will typically show a lower slope than the snowpack, which also possess a lower slope than fresh snow (Lee, Feng, Posmentier, Faiia, & Taylor, 2009; Zhou, Nakawo, Hashimoto, & Sakai, 2008). This could explain why June values in Seeps B and C and in other seeps plot to the left of the LMWL early in the season (late in the season as well for C) as the slope of the seeps ratios (7.4) is significantly lower than the LMWL ( $F$  value 13.8,  $p < .001$ ). This process is caused by fractionation during refreezing in the snowpack (or in the soil), as part of the water is turned back to ice. The residual water ( $\delta_{w,r}$ ) will therefore always plot to the left of the MWL. In our case, the difference between run-off and the LMWL is typically  $<1\%$ . Using Equations 5 and 6 and the average snow signature of  $-28\%$  and  $-220\%$ , this difference would be compensated with a refreezing of  $\leq 30\%$  of the snowmelt water as it travels through the snowpack and the cold soil. Taking into account the average  $\delta^{18}\text{O}$  residuals of the reduced major axis regression used for the LMWL (0.8 ‰), only a small fraction (7%) of the snowmelt needs to be refrozen either in the snowpack or in the soil in order to obtain values that are outside the residual range of the LMWL. High Arctic snowpack can develop substantial ice layer at their base or within the snow layers (Lewkowicz & Young, 1990b; Woo & Heron, 1981), and Marsh and Woo (1984) have demonstrated that between 28% and 46% of the surface melt can refreeze in the snowpack prior to the onset of snowmelt run-off. The required range of 7–30% of refreezing is therefore reasonable, particularly for thick snowdrifts as encountered on the slopes of Walker Hill, or for the predominantly subsurface flows that refreeze in the active layer.

The signature of freeze-out fractionation and evaporative fractionation is sometimes undistinguishable in cold environments (Throckmorton et al., 2016), which brings into question the interpretation of evaporative enrichment based on the isotopic signatures at Seep A. Using Equation 5 with the mean snow signature,

the enriched samples from Seep A (the cluster to the right of the LMWL) also plotted close to the first ice that would have formed after a 10% refreezing of this snow ( $\delta_i = -25.3\%$ ,  $-206.4\%$ )  $\delta_i = -25.3\%$ ,  $-206.4\%$ . However, these samples were from the early melting season, and without a process by which the re-frozen ice would reach the seep before the residual water, they must be interpreted as evaporative enrichment.

The refreezing of snowmelt within the pack causes snowmelt isotopic compositions to show a depleted (more negative) signature early in the season, which leads to the overestimation of snowmelt contributions. This is followed by an enrichment in  $^{18}\text{O}$  and the overestimation of groundwater mixing as the season progresses (Cooper, Solis, Kane, & Hinzman, 1993; Obradovic & Sklash, 1986; Taylor, Feng, Williams, & Mcnamara, 2002). Taylor et al. (2002) used literature values to identify an average increase of the isotopic ratio by 3–5% during the snowmelt season. In our study, the difference between the end member  $\delta^{18}\text{O}$  ratios is only 5.7‰ and would be reduced to 3.2‰ by the end of the season in the case of a 5‰ seasonal increase. Applying such a 3‰ to 5‰ linear correction to the snowmelt average value to the data presented in Figure 7a gives Q1/QT ratios (standard deviation) of 0.58 (0.09) to 0.55 (0.08) for June and 0.46 (0.07) to 0.54 (0.11) for July, compared with original values of 0.64 (0.14) in June and 0.39 (0.05) in July. These corrected values diminish the seasonal variability in snowmelt contribution and the role of groundwater mixing later on.

The percentage of event water yielded by the water track seeps (weighted for discharge) over the entire season was 48% at Seep A and 60% at Seep B. These values are among the highest recorded values for northern catchments according to a compilation by Taylor et al. (2002), where values exceed 50% steadily in only 6 out of 20 studies. They are also higher than values reported for a subarctic watershed, where event water contribution averaged between 10% and 32%, and never reached higher than 55% for a single event (Boucher & Carey, 2010). In Svalbard, only glacier-fed rivers had meltwater steadily dominating the discharge (Blaen, Hannah, Brown, & Milner, 2014), with the rest of the inputs dominated by groundwater. In this polar desert landscape, a combination of nivation processes and soil sorting has allowed the establishment of a drainage pattern dependant on the characteristics and processes of this cold environment, consistent with the cryo-conditioning of cold region landscapes (Berthling & Etzelmüller 2011). Local accumulations of thick snowdrifts dominate snowmelt hydrology, and micromorphology of the slopes and soil organization dictate flow paths and meltwater delivery, together enhancing the structural connectivity of the landscape (Bracken et al., 2013; Bracken & Croke, 2007; Turnbull, Wainwright, & Brazier, 2008). Feedbacks and the effects of flow paths on water quality and on slope evolution remain to be evaluated, but water tracks can act as the dominant carriers of snowmelt water through polar desert slopes. In this particular case, the efficient transfer of water to Ward Hunt Lake is a result of enhanced connectivity between the snowdrifts and the water body. These findings imply that water is rapidly conducted through the slopes with little opportunity for soil–water biogeochemical interactions, which would help explain the low nutrient status of the lake.

## 6 | CONCLUSIONS

Polar desert water tracks in the High Arctic can be efficient downslope carriers of snowmelt. Their run-off generation mechanisms depend on slope profile and on soil organization and are different from the front of a snowdrift, showing some, albeit limited, interaction with the surrounding soils. Early season run-off in the seeping water track networks of Ward Hunt Island was dominated by residual snowmelt water from refreezing snowpack, whereas late season water had the isotopic signature of residual snow, ice and soil water. The water tracks differ from snowdrift seeps, which are dominated by snowmelt water throughout the season. Although seeps dry up once snowdrifts have melted, some seeps were reactivated at the end of a warm summer. These had an isotopic signature that was heavier than active layer ice, towards that of permafrost ice, indicating a possible contribution from the thawing of the ice-rich transient layer. Together, the cold region processes of snowdrift and patterned ground formation have shaped the hydrology of this polar desert slope to enhance downslope connectivity, creating efficient pathways for evacuating water while minimizing interactions with the soil. Defining the hydrological regime of the water tracks draining the western slope of Ward Hunt Lake watershed provides a key step towards linking the limnological conditions of the lake to the characteristics of its watershed.

## ACKNOWLEDGMENTS

This research was conducted with the financial support of the Natural Sciences and Engineering Research Council of Canada (NSERC), including the Discovery Frontiers project Arctic Development and Adaptation to Permafrost in Transition (ADAPT); the Networks of Centres of Excellence program ArcticNet; the Canada Research Chair program; the Northern Scientific Training Program; the Canadian Foundation for Innovation; Canadian Northern Studies Trust; Centre d'études nordiques (CEN); and Fond de Recherche du Québec-Nature et Technologie (FRQNT). Logistical support was provided by the Polar Continental Shelf Program (PCSP) and Parks Canada graciously granted us the use of their facility. The authors would like to thank M. Lafrenière and S. Lamoureux for the use of their facilities, and I. de Grandpré, M. Verpaest, P. Bégin, G. Davesne, and D. Sarrazin for their field assistance as well as two reviewers for their insightful comments and suggestions.

## ORCID

Michel Paquette  <http://orcid.org/0000-0002-5051-7476>

Warwick F. Vincent  <http://orcid.org/0000-0001-9055-1938>

## REFERENCES

- Ball, B. A., & Levy, J. (2015). The role of water tracks in altering biotic and abiotic soil properties and processes in a polar desert in Antarctica. *Journal of Geophysical Research: Biogeosciences*, 120, 270–279. <https://doi.org/10.1002/2014JG002856>
- Berthling, I., & Etzelmüller, B. (2011). The concept of cryo-conditioning in landscape evolution. *Quaternary Research*, 75, 378–384. <https://doi.org/10.1016/j.yqres.2010.12.011>
- Blaen, P. J., Hannah, D. M., Brown, L. E., & Milner, A. M. (2014). Water source dynamics of high Arctic river basins. *Hydrological Processes*, 28, 3521–3538. <https://doi.org/10.1002/hyp.9891>
- Boucher, J. L., & Carey, S. K. G. (2010). Exploring runoff processes using chemical, isotopic and hydrometric data in a discontinuous permafrost catchment. *Hydrology Research*, 41, 508–519. <https://doi.org/10.2166/nh.2010.146>
- Bracken, L. J., & Croke, J. (2007). The concept of hydrological connectivity and its contribution to understanding runoff-dominated geomorphic systems. *Hydrological Processes*, 21, 1749–1763. <https://doi.org/10.1002/hyp.6313>
- Bracken, L. J., Wainwright, J., Ali, G., Tetzlaff, D., Smith, M., Reaney, S., & Roy, A. (2013). Concepts of hydrological connectivity: Research approaches, pathways and future agendas. *Earth-Science Reviews*, 119, 17–34. <https://doi.org/10.1016/j.earscirev.2013.02.001>
- Carey, S. K. (2003). Dissolved organic carbon fluxes in a discontinuous permafrost subarctic alpine catchment. *Permafrost and Periglacial Processes*, 14, 161–171. <https://doi.org/10.1002/ppp.444>
- Carey, S. K., & Quinton, W. L. (2005). Evaluating runoff generation during summer using hydrometric, stable isotope and hydrochemical methods in a discontinuous permafrost alpine catchment. *Hydrological Processes*, 19, 95–114. <https://doi.org/10.1002/hyp.5764>
- Carey, S. K., & Woo, M.-K. (1999). Hydrology of two slopes in subarctic Yukon, Canada. *Hydrological Processes*, 13, 2549–2562. [https://doi.org/10.1002/\(sici\)1099-1085\(199911\)13:16%3C2549::aid-hyp938%3E3.0.co;2-h](https://doi.org/10.1002/(sici)1099-1085(199911)13:16%3C2549::aid-hyp938%3E3.0.co;2-h)
- Carey, S. K., & Woo, M.-K. (2001). Slope runoff processes and flow generation in a subarctic, subalpine catchment. *Journal of Hydrology*, 253, 110–129. [https://doi.org/10.1016/S0022-1694\(01\)00478-4](https://doi.org/10.1016/S0022-1694(01)00478-4)
- CEN. (2016). Climate station data from Northern Ellesmere Island in Nunavut, Canada, v.1.4 (2002–2016). Nordicana D1. <https://doi.org/10.5885/449855L-8F203FD3ACCD4138>
- Cheng, W. X., Virginia, R. A., Oberbauer, S. F., Gillespie, C. T., Reynolds, J. F., & Tenhunen, J. D. (1998). Soil nitrogen, microbial biomass, and respiration along an arctic toposequence. *Soil Science Society of America Journal*, 62, 654–662. <https://doi.org/10.2136/sssaj1998.03615995006200030016x>
- Church, M. (1974). Hydrology and permafrost with reference to northern North America. In *Permafrost hydrology: Proceedings of a workshop seminar* (pp. 7–20). Ottawa, Ontario, Canada: Canadian National Committee, international hydrological decade.
- Cooper, L. W., Solis, C., Kane, D. L., & Hinzman, L. D. (1993). Application of Oxygen-18 tracer techniques to Arctic hydrological processes. *Arctic and Alpine Research*, 25, 247–255.
- Craig, H. (1961). Isotopic variations in meteoric waters. *Science*, 133, 1702–1703. <https://doi.org/10.1126/science.133.3465.1702>
- Curasi, S. R., Loranty, M. M., & Natali, S. M. (2016). Water track distribution and effects on carbon dioxide flux in an eastern Siberian upland tundra landscape. *Environmental Research Letters*, 11, 045002. <https://doi.org/10.1088/1748-9326/11/4/045002>
- Dunne, T., & Black, R. D. (1971). Runoff processes during snowmelt. *Water Resources Research*, 7, 1160–1172. <https://doi.org/10.1029/WR007i005p01160>
- Dunne, T., Moore, T. R., & Taylor, C. H. (1975). Recognition and prediction of runoff-producing zones in humid regions. *Hydrological Sciences Bulletin*, 3, 305–327.
- Dunne, T., Price, A. G., & Colbeck, S. C. (1976). The generation of runoff from subarctic snowpacks. *Water Resources Research*, 12, 677–685. <https://doi.org/10.1029/WR012i004p0677>
- Genereux, D. (1998). Quantifying uncertainty in tracer-based hydrograph separations. *Water Resources Research*, 34, 915–919. <https://doi.org/10.1029/98WR00010>
- Gooseff, M. N., Barrett, J. E., & Levy, J. S. (2013). Shallow groundwater systems in a polar desert, McMurdo Dry Valleys, Antarctica. *Hydrogeology Journal*, 21, 171–183. <https://doi.org/10.1007/s10040-012-0926-3>
- Hamlin, L., Pietroniro, A., Prowse, T., Soulis, R., & Kouwen, N. (1998). Application of indexed snowmelt algorithms in a northern wetland regime. *Hydrological Processes*, 12, 1641–1657. <https://doi.org/10.1002/>

- (sici)1099-1085(199808/09)12:10/11%3C1641::aid-hyp686%3E3.0.co;2-w
- Hardy, D. R. (1996). Climatic influences on streamflow and sediment flux into Lake C2, northern Ellesmere Island, Canada. *Journal of Paleolimnology*, 16, 133–149. <https://doi.org/10.1007/BF00176932>
- Harris, K. J., Carey, A. E., Lyons, W. B., Welch, K. A., & Fountain, A. G. (2007). Solute and isotope geochemistry of subsurface ice melt seeps in Taylor Valley, Antarctica. *Geological Society of America Bulletin*, 119, 548–555. <https://doi.org/10.1130/b25913.1>
- Hastings, S. J., Luchessa, S. A., Oechel, W. C., & Tenhunen, J. D. (1989). Standing biomass and production in water drainages of the foothills of the Philip Smith Mountains, Alaska. *Holarctic Ecology*, 12, 304–311. <https://doi.org/10.1111/j.1600-0587.1989.tb00850.x>
- Hodgson, R., & Young, K. L. (2001). Preferential groundwater flow through a sorted net landscape, Arctic Canada. *Earth Surface Processes and Landforms*, 26, 319–328. [https://doi.org/10.1002/1096-9837\(200103\)26:3%3C319::AID-ESP176%3E3.0.CO;2-1](https://doi.org/10.1002/1096-9837(200103)26:3%3C319::AID-ESP176%3E3.0.CO;2-1)
- Hoffman, M. J., Fountain, A. G., & Liston, G. E. (2014). Near-surface internal melting: A substantial mass loss on Antarctic Dry Valley glaciers. *Journal of Glaciology*, 60, 361–374. <https://doi.org/10.3189/2014Jog13J095>
- International Atomic Energy Agency/World Meteorological Organization. (2017). Global network of isotopes in precipitation. The GNIP Database. <http://www.iaea.org/water>.
- Kane, D. L., Hinzman, L. D., Benson, C. S., & Liston, G. E. (1991). Snow hydrology of a headwater Arctic basin. 1. Physical measurements and process studies. *Water Resources Research*, 27(6), 1099–1109. <https://doi.org/10.1029/91WR00262>
- Lacelle, D. (2011). On the  $\delta^{18}O$ ,  $\delta D$  and D-excess relations in meteoric precipitation and during equilibrium freezing: Theoretical approach and field examples. *Permafrost and Periglacial Processes*, 22, 13–25. <https://doi.org/10.1002/ppp.712>
- Lamhonwah, D., Lafrenière, M. J., Lamoureux, S. F., & Wolfe, B. B. (2017). Evaluating the hydrological and hydrochemical responses of a High Arctic catchment during an exceptionally warm summer. *Hydrological Processes*, 31, 2296–2313. <https://doi.org/10.1002/hyp.11191>
- Lee, J., Feng, X., Posmentier, E. S., Faiia, A. M., & Taylor, S. (2009). Stable isotopic exchange rate constant between snow and liquid water. *Chemical Geology*, 260, 57–62. <https://doi.org/10.1016/j.chemgeo.2008.11.023>
- Lemmen, D. S. (1988). The glacial history of Marvin Peninsula, Northern Ellesmere Island, and Ward Hunt Island, High Arctic Canada. (Ph.D. thesis), University of Alberta, Edmonton, Canada, 176 p.
- Lemmen, D. S., & England, J. (1992). Multiple glaciations and sea level changes, northern Ellesmere Island, High Arctic Canada. *Boreas*, 21, 137–152. <https://doi.org/10.1111/j.1502-3885.1992.tb00021.x>
- Levy, J. S., Fountain, A. G., Gooseff, M. N., Welch, K. A., & Lyons, W. B. (2011). Water tracks and permafrost in Taylor Valley, Antarctica: Extensive and shallow groundwater connectivity in a cold desert ecosystem. *Geological Society of America Bulletin*, 123, 2295–2311. <https://doi.org/10.1130/b30436.1>
- Levy, J. S., & Schmidt, L. M. (2016). Thermal properties of Antarctic soils: Wetting controls subsurface thermal state. *Antarctic Science*, 28, 361–370. <https://doi.org/10.1017/S0954102016000201>
- Lewkowicz, A. G., & French, H. M. (1982). The hydrology of small runoff plots in an area of continuous permafrost, Banks Island, N.W.T. In H. M. French (Ed.), *Proceedings of the 4th Canadian Permafrost Conference* (pp. 151–162). Calgary, Alberta, Canada: National Research Council of Canada.
- Lewkowicz, A. G., & Young, K. L. (1990a). Hydrological processes in a small catchment containing a perennial snowbank, Melville Island, N.W.T. In T. D. Prowse, & C. S. L. Ommaney. (Eds.), *Northern Hydrology, Selected Perspectives, Proceedings of the NHRI Symposium No. 6* (pp. 237–251). Saskatoon, Saskatchewan, Canada: National Hydrology Research Institute.
- Lewkowicz, A. G., & Young, K. L. (1990b). Hydrology of a perennial snowbank in the continuous permafrost zone, Melville Island, Canada. *Geografiska Annaler. Series A, Physical Geography*, 72, 13–21. <https://doi.org/10.2307/521234>
- Marsh, P., & Woo, M.-K. (1984). Wetting front advance and freezing of meltwater within a snow cover: 1. Observations in the Canadian Arctic. *Water Resources Research*, 20, 1853–1864. <https://doi.org/10.1029/WR020i012p01853>
- Mcnamara, J. P., Kane, D. L., & Hinzman, L. D. (1998). An analysis of streamflow hydrology in the Kuparuk River Basin, Arctic Alaska: A nested watershed approach. *Journal of Hydrology*, 206, 39–57. [https://doi.org/10.1016/S0022-1694\(98\)00083-3](https://doi.org/10.1016/S0022-1694(98)00083-3)
- Mcnamara, J. P., Kane, D. L., & Hinzman, L. D. (1999). An analysis of an arctic channel network using a digital elevation model. *Geomorphology*, 29, 339–353. [https://doi.org/10.1016/S0169-555X\(99\)00017-3](https://doi.org/10.1016/S0169-555X(99)00017-3)
- Mcnamara, J. P., Kane, D. L., Hobbie, J. E., & Kling, G. W. (2008). Hydrologic and biogeochemical controls on the spatial and temporal patterns of nitrogen and phosphorus in the Kuparuk River, Arctic Alaska. *Hydrological Processes*, 22, 3294–3309. <https://doi.org/10.1002/hyp.6920>
- Nicholson, F. (1978). Permafrost distribution and characteristics near Schefferville, Quebec: Recent studies. In R. J. E. Brown (Ed.), *Proceedings of the 3rd international conference on permafrost* (pp. 427–433). Edmonton, Alberta, Canada: National Research Council of Canada.
- Oberbauer, S. F., Tenhunen, J. D., & Reynolds, J. F. (1991). Environmental effects on CO<sub>2</sub> efflux from water track and tussock tundra in Arctic Alaska, U.S.A. *Arctic and Alpine Research*, 23, 162–169. <https://doi.org/10.2307/1551380>
- Obradovic, M. M., & Sklash, M. G. (1986). An isotopic and geochemical study of snowmelt runoff in a small arctic watershed. *Hydrological Processes*, 1, 15–30. <https://doi.org/10.1002/hyp.3360010104>
- O'neil, J. R. (1968). Hydrogen and oxygen isotope fractionation between ice and water. *The Journal of Physical Chemistry*, 72, 3683–3684. <https://doi.org/10.1021/j100856a060>
- Paquette, M., Fortier, D., Mueller, D. R., Sarrazin, D., & Vincent, W. F. (2015). Rapid disappearance of perennial ice on Canada's most northern lake. *Geophysical Research Letters*, 42, 1433–1440. <https://doi.org/10.1002/2014GL062960>
- Paquette, M., Fortier, D., & Vincent, W. F. (2017). Water tracks in the High Arctic: A hydrological network dominated by rapid subsurface flow through patterned ground. *Arctic Science*, 3, 334–353. <https://doi.org/10.1139/as-2016-0014>
- Quesada, A., Vincent, W. F., Kaup, E., Hobbie, J. E., Laurion, I., Pienitz, R., ... Durán, J. J. (2006). Landscape control of high Latitude Lakes in a changing climate. In D. M. Bergstrom, P. Convey, & A. H. L. Huiskes (Eds.), *Trends in Antarctic Terrestrial and Limnetic Ecosystems* (pp. 221–252). Dordrecht, Netherlands: Springer.
- Quinton, W. L., Carey, S. K., & Goeller, N. T. (2004). Snowmelt runoff from northern alpine tundra hillslopes: Major processes and methods of simulation. *Hydrology and Earth System Sciences*, 8, 877–890. <https://doi.org/10.5194/hess-8-877-2004>
- Quinton, W. L., Gray, D. M., & Marsh, P. (2000). Subsurface drainage from hummock-covered hillslopes in the Arctic tundra. *Journal of Hydrology*, 237, 113–125. [https://doi.org/10.1016/S0022-1694\(00\)00304-8](https://doi.org/10.1016/S0022-1694(00)00304-8)
- Quinton, W. L., & Marsh, P. (1998). The influence of mineral earth hummocks on subsurface drainage in the continuous permafrost zone. *Permafrost and Periglacial Processes*, 9, 213–228. [https://doi.org/10.1002/\(SICI\)1099-1530\(199807/09\)9:3%3C213::AID-PPP285%3E3.0.CO;2-E](https://doi.org/10.1002/(SICI)1099-1530(199807/09)9:3%3C213::AID-PPP285%3E3.0.CO;2-E)
- Quinton, W. L., & Marsh, P. (1999). A conceptual framework for runoff generation in a permafrost environment. *Hydrological Processes*, 13, 2563–2581. [https://doi.org/10.1002/\(sici\)1099-1085\(199911\)13:16%3C2563::aid-hyp942%3E3.0.co;2-d](https://doi.org/10.1002/(sici)1099-1085(199911)13:16%3C2563::aid-hyp942%3E3.0.co;2-d)
- R Core Team (2014). *R: A language and environment for statistical computing*. Vienna, Austria: R foundation for statistical computing. <http://www.r-project.org/>
- Roesch, A., & Schmidbauer, H. (2014). WaveletComp: Computational wavelet analysis. R package version 1.0. <http://cran.r-project.org/package=WaveletComp>.

- Rushlow, C. R., & Godsey, S. E. (2017). Rainfall-runoff responses on Arctic hillslopes underlain by continuous permafrost, north slope, Alaska, USA. *Hydrological Processes*, 31, 4092–4106. <https://doi.org/10.1002/hyp.11294>
- Shur, Y. (1988). The upper horizon of permafrost soils. In K. Senneset (Ed.), *Proceedings of the fifth international conference on permafrost* (pp. 867–871). Trondheim, Norway.
- Shur, Y., Hinkel, K. M., & Nelson, F. E. (2005). The transient layer: Implications for geocryology and climate-change science. *Permafrost and Periglacial Processes*, 16, 5–17. <https://doi.org/10.1002/ppp.518>
- Siddiqui, R., Lashari, B., & Skogerboe, G. V. (1996). Converting a fabricated cutthroat flume into a discharge measuring instrument. (T-5). Hyderabad Office: Pakistan National Program International Irrigation Management Institute.
- Sklash, M. G., & Farvolden, R. N. (1979). The role of groundwater in storm runoff. *Journal of Hydrology*, 12, 45–65. [https://doi.org/10.1016/S0167-5648\(09\)70009-7](https://doi.org/10.1016/S0167-5648(09)70009-7)
- Taylor, S., Feng, X., Williams, M., & Mcnamara, J. (2002). How isotopic fractionation of snowmelt affects hydrograph separation. *Hydrological Processes*, 16, 3683–3690. <https://doi.org/10.1002/hyp.1232>
- Throckmorton, H. M., Newman, B. D., Heikoop, J. M., Perkins, G. B., Feng, X., Graham, D. E., ... Wilson, C. J. (2016). Active layer hydrology in an arctic tundra ecosystem: Quantifying water sources and cycling using water stable isotopes. *Hydrological Processes*, 30, 4972–4986. <https://doi.org/10.1002/hyp.10883>
- Trettin, H. P. (1991). *Geology of the Innuitian Orogen and Arctic Platform of Canada and Greenland. Geological Survey of Canada, Geology of Canada Series*. no. 3, (p. 569). <https://doi.org/10.4095/133959>
- Turnbull, L., Wainwright, J., & Brazier, R. E. (2008). A conceptual framework for understanding semi-arid land degradation: Ecohydrological interactions across multiple-space and time scales. *Ecohydrology*, 1, 23–34. <https://doi.org/10.1002/eco.4>
- Verpaelst, M., Fortier, D., Kanevskiy, M., Paquette, M., & Shur, Y. (2017). Syngenetic dynamic of permafrost of a polar desert solifluction lobe, Ward Hunt Island, Nunavut. *Arctic Science*, 3, 301–319. <https://doi.org/10.1139/as-2016-0018>
- Villeneuve, V., Vincent, W. F., & Komárek, J. (2001). Community structure and microhabitat characteristics of cyanobacterial mats in an extreme high Arctic environment: Ward Hunt Lake. *Nova Hedwigia. Beiheft*, 123, 199–224.
- Vincent, W. F., Fortier, D., Lévesque, E., Boulanger-Lapointe, N., Tremblay, B., Sarrazin, D., ... Mueller, D. R. (2011). Extreme ecosystems and geosystems in the Canadian High Arctic: Ward Hunt Island and vicinity. *Ecoscience*, 18, 236–261. <https://doi.org/10.2980/18-3-3448>
- Whiting, P. J. (2005). Flow measurement and characterization. In G. M. Kondolf, & H. Piégay (Eds.), *Tools in fluvial geomorphology* (pp. 323–346). Chichester, England: John Wiley & Sons, Ltd.
- Woo, M.-K. (1983). Hydrology of a drainage basin in the Canadian High Arctic. *Annals of the Association of American Geographers*, 73, 577–596.
- Woo, M.-K., & Heron, R. (1981). Occurrence of ice layers at the base of High Arctic snowpacks. *Arctic and Alpine Research*, 13, 225–230.
- Woo, M.-K., Heron, R., & Steer, P. (1981). Catchment hydrology of a High Arctic lake. *Cold Regions Science and Technology*, 5, 29–41. [https://doi.org/10.1016/0165-232x\(81\)90038-0](https://doi.org/10.1016/0165-232x(81)90038-0)
- Woo, M.-K., & Steer, P. (1983). Slope hydrology as influenced by thawing of the active layer, resolute, N.W.T. *Canadian Journal of Earth Sciences*, 20, 978–986. <https://doi.org/10.1139/e83-087>
- Woo, M.-K., & Xia, Z. (1995). Suprapermfrost groundwater seepage in gravelly terrain, Resolute, NWT, Canada. *Permafrost and Periglacial Processes*, 6, 57–72. <https://doi.org/10.1002/ppp.3430060107>
- Woo, M.-K., Yang, D., & Young, K. L. (1999). Representativeness of arctic weather station data for the computation of snowmelt in a small area. *Hydrological Processes*, 13, 1859–1870. [https://doi.org/10.1002/\(sici\)1099-1085\(199909\)13:12<13%3C1859::aid-hyp893%3E3.0.co;2-d](https://doi.org/10.1002/(sici)1099-1085(199909)13:12<13%3C1859::aid-hyp893%3E3.0.co;2-d)
- Woo, M.-K., Yang, Z., Xia, Z., & Yang, D. (1994). Streamflow processes in an alpine permafrost catchment, Tianshan, China. *Permafrost and Periglacial Processes*, 5, 71–85. <https://doi.org/10.1002/ppp.3430050202>
- Woo, M.-K., & Young, K. L. (2003). Hydrogeomorphology of patchy wetlands in the High Arctic, polar desert environment. *Wetlands*, 23, 291–309. <https://doi.org/10.1672/8-20>
- Young, K. L., & Lewkowicz, A. G. (1990). Surface energy balance of a perennial snowbank, Melville Island, Northwest Territories, Canada. *Arctic and Alpine Research*, 22, 290–301. <https://doi.org/10.2307/1551592>
- Young, K. L., Woo, M.-K., & Edlund, S. A. (1997). Influence of local topography, soils, and vegetation on microclimate and hydrology at a High Arctic site, Ellesmere Island, Canada. *Arctic and Alpine Research*, 29, 270–284. <https://doi.org/10.2307/1552141>
- Zhou, S., Nakawo, M., Hashimoto, S., & Sakai, A. (2008). The effect of refreezing on the isotopic composition of melting snowpack. *Hydrological Processes*, 22, 873–882. <https://doi.org/10.1002/hyp.6662>

**How to cite this article:** Paquette M, Fortier D, Vincent WF. Hillslope water tracks in the High Arctic: Seasonal flow dynamics with changing water sources in preferential flow paths. *Hydrological Processes*. 2018;1–13. <https://doi.org/10.1002/hyp.11483>